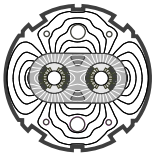

LHC Project Note 250

01. March 2001

Diffusive Aperture due to Long-Range Collisions at Injection and Image-Charge Effects

F. Zimmermann, CERN, Geneva, Switzerland

Keywords: beam-beam interaction, parasitic collisions, dynamic aperture, image charge

Summary

We study the LHC diffusive aperture induced by long-range collisions at injection and the effect of image charges at the parasitic collision points, by means of a weak-strong computer simulation. Expressed in terms of beam size, for a constant normalized beam-beam separation the diffusive aperture is shown to be independent of the IP beta function and the beam energy. The effect of image charges is proven negligible.

1 Introduction

Simplified tracking studies [1, 2] have shown that for the nominal LHC parameters the long-range parasitic collisions give rise to a well-defined diffusive aperture. At top energy the diffusive aperture corresponds to a simultaneous amplitude in both planes of about 5.5σ (or $\sqrt{2}$ times this number in terms of radial distance to the origin). Outside this aperture the particle motion is chaotic and particles are eventually lost, if nonlinear magnetic fields in the low-β quadrupoles are also included. The strong degradation of the dynamic aperture by the parasitic collisions has been confirmed in more precise simulations which accurately model the individual parasitic collision points [3]. The first part of this paper examines how the value of the diffusive aperture depends on beam energy and optics, *e.g.*, β squeeze. In the second part we address the question whether the effect of the long-range collision is possibly alleviated by the image charges of the opposite beam.

2 Long-Range Beam-Beam Effects at Injection

2.1 Scaling Consideration

In our model [2] the long-range forces from all parasitic encounters on one side of each interaction point (IP) are lumped together into a single kick, placed at a betatron phase distance of 90° from

the interaction point, ignoring the small betatron phase advance between the different parasitic collision points. If the particle position is at least 2 or 3 rms beam sizes away from the center of the opposing beam, this total kick, expressed as a shift in the coordinate at the primary IP, can be approximated, for horizontal crossing, as

$$\begin{aligned} \Delta x &\approx -n_{\rm par}\,\frac{2r_pN_b}{\gamma}\,\left[\frac{x'+\theta_c}{\theta_t^2}-\frac{1}{\theta_c}\right] \\ \Delta y &\approx -n_{\rm par}\,\frac{2r_pN_b}{\gamma}\,\frac{y'}{\theta_t^2}, \end{aligned} \tag{1}$$

where $\theta_t \equiv \left((x'+\theta_c)^2+y'^2\right)^{1/2}$, θ_c denotes the full crossing angle, x' the horizontal slope of the particle trajectory at the collision point, y' the vertical slope, N_b the bunch population, γ the beam energy in units of the rest mass, and $n_{\rm par}$ the number of parasitic collisions on one side of the IP. In the following, we take $n_{\rm par}$ conservatively as equal to 18, although 2 of these parasitic encounters occur at such large distances that they could be ignored [4]. In the first part of Eq. (1), we subtracted the average horizontal dipole kick on the bunch, since its effect would be corrected by steering correctors. Note that the kick is the same on both sides of the IP, because the betatron phase advance of about 180° compensates for the opposite direction of the beam-beam separation. The vertical crossing is treated in complete analogy.

Considering the simplified case of 1-dimensional motion, $y'=0$, we may expand the first row of Eq. (1) as

$$\Delta x \approx -n_{\rm par}\,\frac{2r_pN_b}{\gamma}\,\left[-\frac{x'}{\theta_c^2}+\frac{x'^2}{\theta_c^3}+\ldots\right] = n_{\rm par}\,\frac{2r_pN_b}{\gamma}\,\sum_m (-1)^m\,\frac{x'^m}{\theta_c^{m+1}} \tag{2}$$

We now consider a single term in the expansion on the right-hand side. We recall that a trajectory slope x' at the IP with zero offset corresponds to a betatron-oscillation amplitude of $x=\beta_x^* x'$ at the IP. To get a rough estimate, we assume that the onset of chaoticity occurs for a certain magnitude of the relative perturbation $\Delta x/x$. This condition for the diffusive aperture $x_{\rm da}$ can be approximated as

$$\left|\frac{\Delta x}{x_{\rm da}}\right| \approx n_{\rm par}\frac{2r_pN_b}{\gamma}\,\frac{{x'_{\rm da}}^{m-1}}{\theta_c^{m+1}} \approx \text{constant}. \tag{3}$$

Solving the right-hand side of this equation for $x'_{\rm da}$ and expressing the diffusive aperture normalized to the rms beam size by $x_{\rm da}/\sigma_x = x'_{\rm da}\beta_x^*/\sigma_x$, we find that the latter should scale as

$$\frac{x_{\rm da}}{\sigma_x} \sim \left[\frac{\epsilon_N n_{\rm sep}^2}{n_{\rm par}N_b}\right]^{\frac{1}{m-1}}\,n_{\rm sep}, \tag{4}$$

where $n_{\rm sep}$ denotes the ratio of the full crossing angle to the rms IP divergence, $\epsilon_N=\gamma\epsilon$ the normalized transverse emittance, $\sigma_x=\sqrt{\epsilon\beta_x^*}$ the rms IP beam size, and $\theta_c = n_{\rm sep}\sqrt{\epsilon/\beta_x^*}$. Note that higher-order terms with $m \gg 1$ will be important, since the lowest-order effects can be corrected by the optics, *e.g.*, by the choice of working point.

Equation (4) suggests that the diffusive aperture is independent of IP beta function and beam energy. It depends, however, on the normalized emittance, the bunch population, the number of parasitic encounters, and, especially, the beam-beam separation. In order to verify this scaling, we have performed a series of weak-strong simulations using the model described in Ref. [2].

2.2 Simulation Results

The diffusive aperture due to long-range collisions depends on the separation of the two beams at the parasitic collision points, and thus essentially on the ratio of the crossing angle to the rms beam divergence [1, 8]. In the present LHC optics design, the average beam-beam separation at top energy is about 10 σ ($n_{\rm sep} = 10$) around all 4 LHC interaction points, while at injection it is larger, about 14 σ ($n_{\rm sep} = 14$) [5]. For our simulation we have assumed a 10-σ separation in either case, for two reasons: (1) at the time of the study the exact magnitude of separation at injection had not yet been decided, and (2) we were interested in the general scaling of the diffusive aperture with beam energy and IP beta function, maintaining a constant beam-beam separation in units of the rms beam size.

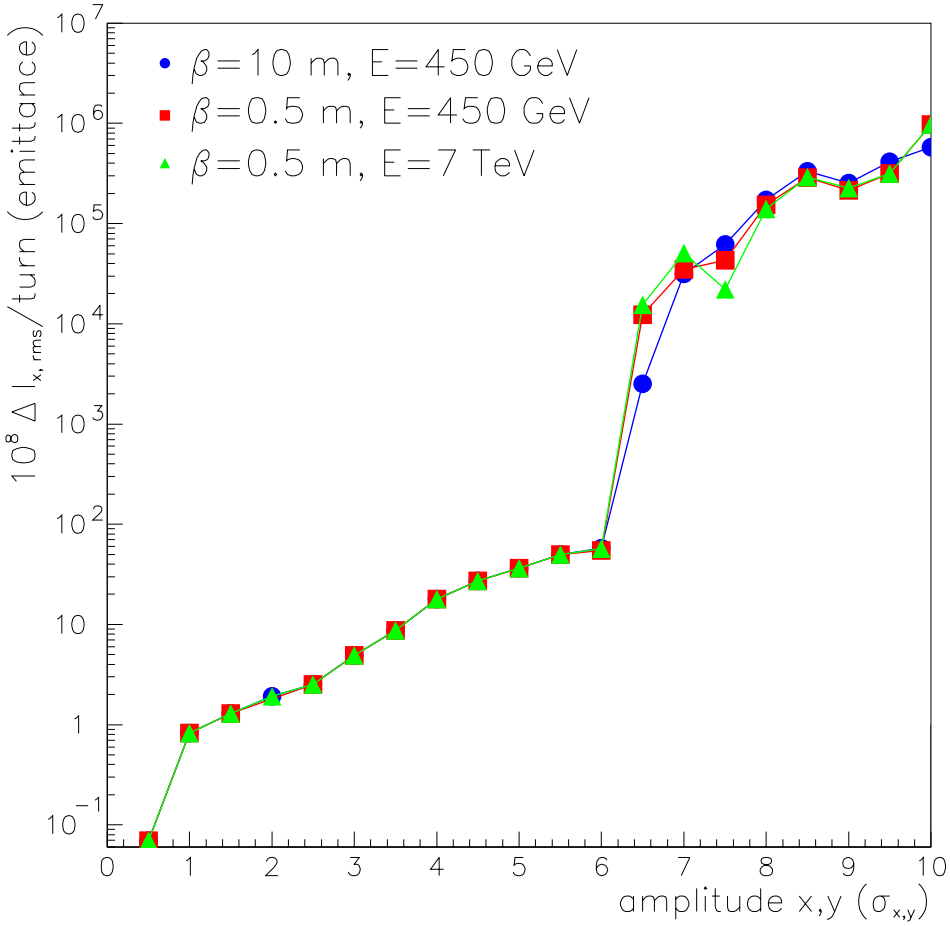

Figure 1: Simulated action diffusion rates as a function of starting amplitude, for two different values of β^* and the beam energy; other parameters were chosen as $\epsilon_N = 3.75$ μm, energy 450 GeV, $n_{\rm sep} = 10$, and $n_{\rm par} = 18$ on either side of 2 IPs with alternating crossing, for the working point $Q_x = 0.31$ and $Q_y = 0.32$.

Figure 1 compares simulated diffusion rates (characterized in terms of the growth in the rms spread of action per turn divided by the rms design emittance [2]) as a function of normalized starting amplitude, for a situation with only two interaction points. At oscillation amplitudes of about 7σ (or $n_{\rm sig} = 7$), a value of $10^6\epsilon/(10^8{\rm turns})$ is found for the diffusion coefficient plotted along the vertical axis. This means that the spread of the squared particle amplitudes increases by an amount equal to the nominal rms beam emittance after 100 turns ($= 10^8/10^6$). The amplitude doubling time would be $n_{\rm sig}^2$ times larger or 5000 turns. In other words, beyond 6σ the diffusion is so strong that many particles are lost in less than 10^4 turns. Figure 1 illustrates that the simulation nicely confirms the insensitivity to β^* and γ expected from Eq. (4).

We next extended the number of interaction points to 4. At the time these simulations were conducted, the crossing schemes at interaction points 2 and 8 had not yet been definitely determined. In the present scheme [6, 7], at two of the four LHC interaction points the beams cross in the vertical plane, at the other two in the horizontal plane. This miminizes the total tune shifts induced by the long-range encounters. If, on the other hand, for three of the collision points the crossings were to take place in the vertical plane, and only at one IP in the horizontal plane, the linear tune shifts induced by the different long-range encounters would not cancel, and, as a result, the diffusive aperture measured in units of the rms beam size would be smaller than in collision.

This question is illuminated in Fig. 2, which compares the simulated diffusion rates at injection energy for different situations:

- two IPs with 18 parasitic encounters per side per IP, all assumed with a 10 σ separation
- two IPs with twice the number of parasitic collisions to approximate the effect of 4 IPs,
- four IPs with 1 vertical and 3 horizontal crossings
- 4 IPs with 18 parasitic collisions and perfect alternating crossing and
- four IPs with 1 horizontal and 3 vertical crossings

In all cases, the working point was set to $Q_x = 0.31$, $Q_y = 0.32$, which corresponds to the nominal tunes in collision. In one of the partial crossing schemes (case 3, *i.e.*, 3 horizontal and 1 vertical crossing), there is enhanced diffusion already at 2 σ. On the other hand, for three vertical and 1 horizontal crossings (case 5 in Fig. 2), the diffusion is slightly reduced. Exchanging the horizontal and vertical working points reverses the situation.

Figure 3 illustrates the dependence on the number of parasitic encounters per side and per IP, $n_{\rm par}$. Diffusion rates are shown for different values of $n_{\rm par}$, assuming 4 LHC interaction points, 3 of which with vertical crossings and the last with horizontal crossing. The left picture refers to the collision tunes ($Q_x = 0.31$, $Q_y = 0.32$). The right picture depicts the corresponding results for the injection tunes ($Q_x = 0.28$, $Q_y = 0.31$). The figure demonstrates that, if there are fewer close-by parasitic encounters, the diffusive aperture increases. Its distance to the opposing beam decreases roughly as $\sqrt{n_{\rm par}}$. For example, with ten parasitic encounters at 10σ, the diffusive aperture is about 7.5σ, with 5 parasitic encounters it is 8.5σ, and for only two parasitic encounters, we find the diffusive aperture at about 10σ, *i.e.*, where particles start passing through the center of the other beam.

Our intermediate conclusion is that if the number of parasitic encounters $n_{\rm par}$ and the separation in units of the rms beam size, $n_{\rm sep}$, were about the same as in collisions, the long-range beam-beam

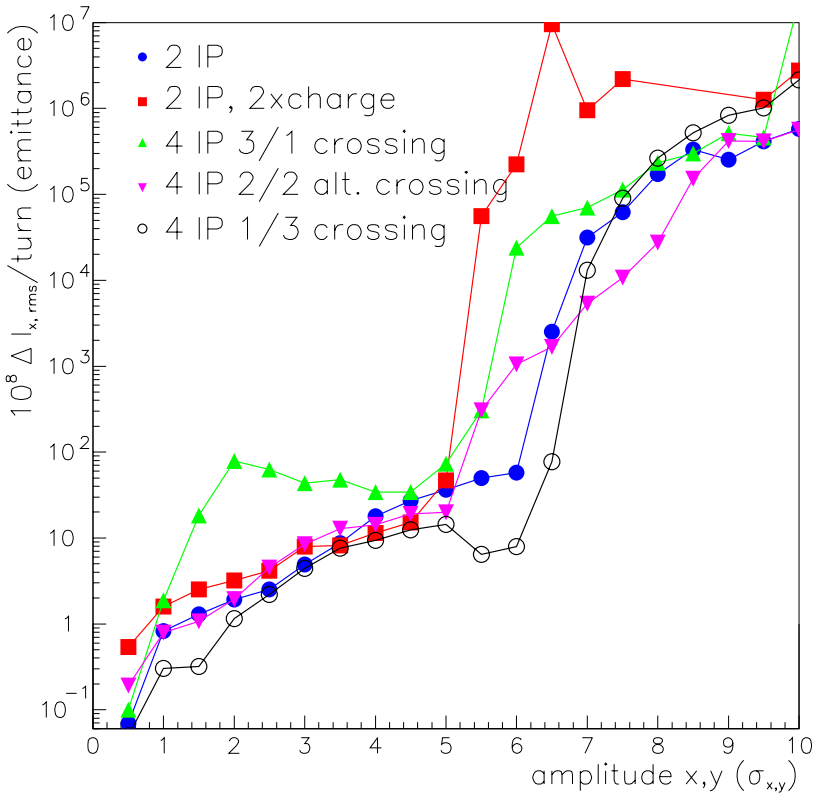

Figure 2: Simulated action diffusion rates as a function of starting amplitude, for different number of IPs, parasitic collision points (or charge), and different crossing schemes, for the fractional tunes $Q_x = 0.31$ and $Q_y = 0.32$ (nominal working point in collision); other parameters were chosen as $\epsilon_N = 3.75$ μm, energy 450 GeV, $n_{\rm sep} = 10$, and $n_{\rm par} = 18$.

encounters would induce a similar diffusive aperture of about 6σ also at injection. In particular, the diffusive aperture is independent of beam energy and IP beta function. In the present injection scheme, the average separation is about 50% larger than in collision, and, therefore, the diffusive aperture due to the long-range collisions at injection will be larger by a similar factor and close to 9σ.

3 Image-Charge Effect

3.1 Model

The weak-strong simulation model of Ref. [1, 2] can easily be extended so as to include the effect of image charges induced by the opposing beam on the long-range beam-beam interaction.

To derive the additional kick due the image charge consider first a line charge λ at a distance a from the center of a cylinder of radius b. The conducting boundary conditions are fulfilled by placing an image charge $-\lambda$ at a radius b^2/a. The translation to our problem is rather straightfor-

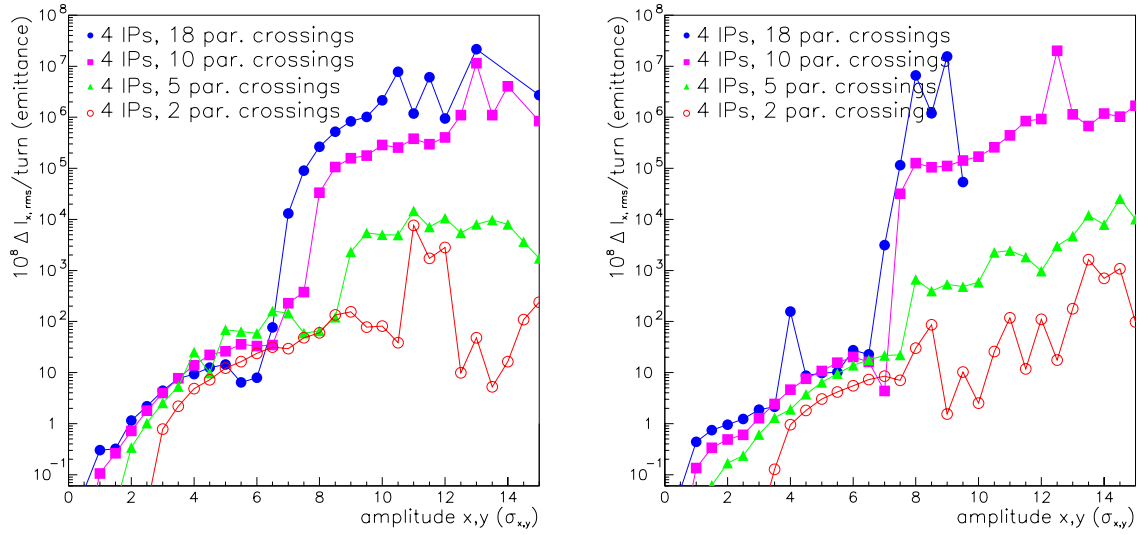

Figure 3: Simulated action diffusion rates as a function of starting amplitude, for different numbers of parasitic encounters at 10σ, assuming 4 interaction points, 1 horizontal and 3 vertical crossings, and either the nominal tunes for collisions, $Q_x = 0.31$ and $Q_y = 0.32$ [left] or the injection tunes $Q_x = 0.28$ and $Q_y = 0.31$ [right].

ward. For simplicity, in the calculation of the image-charge force we ignore the finite transverse size of the source beam. To represent the image charge, we apply a kick as in Eq. (1), but of opposite sign and with θ_c replaced by the angular distance (*i.e.*, the spatial distance at the collision point translated into IP phase-space coordinates) between the center of the test beam and the image charge,

$$\theta_{c,\mathrm{im}} = 2\,\frac{\theta_\phi^2}{\theta_c} + \frac{\theta_c}{2}, \tag{5}$$

where

$$\theta_\phi = \frac{b}{\sqrt{\beta_x^*\beta_{x,b}}\,\sin\Delta\phi} \approx \frac{b}{\sqrt{\beta_x^*\beta_{x,b}}} \tag{6}$$

with b the radial aperture, $\beta_{x,b}$ the beta function at the location of the long-range collision and $\Delta\phi \approx \pi/2$ the betatron phase advance between the IP and the parasitic collision point. In Eq. (5), the term θ_ϕ^2 corresponds to the square of the beam-pipe radius at the parasitic collision point, b^2, and the term $\theta_c/2$ to the local offset a of the opposite beam from the center of the chamber, both translated into equivalent angles at the IP. The last term, $\theta_c/2$, represents the orbit offset of the probe beam from the beam-pipe center, again converted into an IP angle. If there are no quadrupoles between the collision point and the IP, we may also write $\theta_\phi \approx b/l_b$ with l_b the distance to the IP. More generally, we have $\theta_\phi \approx b/a\;(\theta_c/2)$. In Eq. (5), we have assumed that the beams are displaced symmetrically with respect to the center of the chamber, which is only approximately correct for the parasitic collision points inside and upstream of the low-beta quadrupoles.

Explicitly, the formula for the image-charge kick reads

$$\begin{aligned} \Delta x &= n_{\rm par}\,\frac{2r_pN_b}{\gamma}\,\left[\,\frac{x'+\theta_{c,\rm im}}{\theta^2_{t,\rm im}}\,-\frac{1}{\theta_c}\right] \\ \Delta y &= n_{\rm par}\,\frac{2r_pN_b}{\gamma}\,\frac{y'}{\theta^2_{t,\rm im}}, \end{aligned} \tag{7}$$

where $\theta_{t,\rm im}\equiv\left((x'+\theta_{c,\rm im})^2+y'^2\right)^{1/2}$.

3.2 Results

As an example, taking $b=24$ mm and $l_b=23$ m, we obtain $\theta_\phi=1$ mrad, and $\theta_{c,\rm im}\approx 7.4$ mrad. The angle $\theta_{c,\rm im}$ is more than 20 times larger than the crossing angle $\theta_c\approx 300$ μrad. For this reason, we may expect that the image charge effect will be small, if not negligible. Figure 4 depicts the kick Δx as a function of x' with and without the image charge, for various beam offsets. Even considering, for *all* parasitic collision points, the maximum beam offset of 9 mm at a radial aperture of 3 cm, in reality occuring at one location inside the final triplet, the effect of the image-charge force is still small. For these values as well as for $a=3$ mm and $b=24$ mm, the effect of the image charge is visible only in a close-up view, illustrated in the right picture. The beam-beam force is substantially reduced by the image charges only for beam offsets approaching the chamber radius b, *e.g.*, for $a=20$ mm and $a=25$ mm in Fig. 4. Thus only in those cases we would expect the image charges to affect the diffusive aperture.

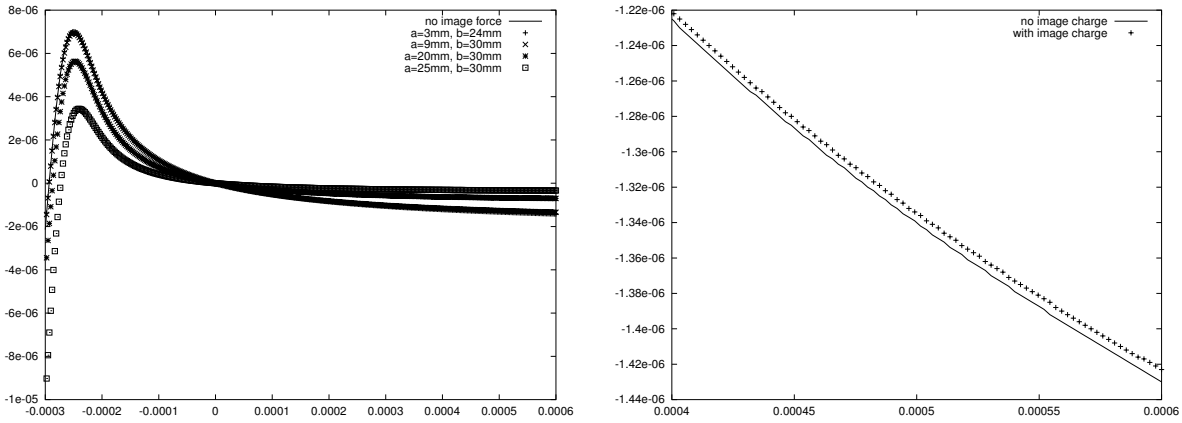

Figure 4: Left: Long-range beam-beam kick Δx, in m, as a function of x', in rad, with and without including the effect of image charges, Eq. (7), for various beam offsets and chamber radii. Right: A close-up view for $\theta_\phi=1$ mrad (offset of $a=3.5$ mm at $b=24$ mm), $\theta_c=300$ μrad, $N_b=1.05\times10^{11}$, and $\gamma=7461$, revealing a small difference. when image charge is included.

In order to verify this expectation, we have performed weak-strong simulations at top energy both with and without the image-charge effect. In these simulations we included collisions at 2 IPs, and, for the image charge calculation, we assumed the worst-case parameters listed above, for *all* parasitic collision points. The resulting action-diffusion rates for various beam offsets and

chamber apertures are compared in Fig. 5, as a function of starting amplitude. As already expected from Fig. 4, the effect of the image charge becomes visible only for offsets a larger than half the chamber radius, where, for a equal to 2 cm or 2.5 cm and a chamber radius of 3 cm they increase the diffusive aperture by about 0.5σ.

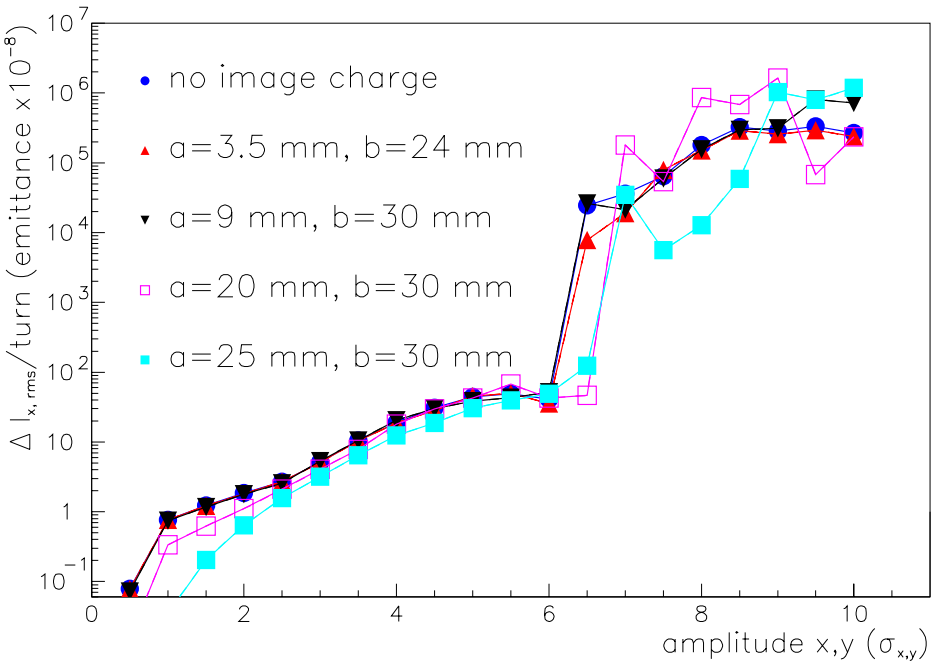

Figure 5: Change of action variance per turn, in units of the rms beam emittance, as a function of the starting amplitude in units of σ. Compared are simulation results with and without image charges at the long-range collision points.

4 Summary

If quoted in units of the rms beam size, the diffusive apertures at injection and top energy are comparable for the same normalized beam-beam separation. In particular, the diffusive aperture is independent of β^* and beam energy. However, it does strongly depend on the number of parasitic encounters, on the betatron tunes, and on the crossing schemes at the various IPs. For the present design values of beam displacements and chamber radii, the effect of image-charge forces at the parasitic collision points is negligible.

Acknowledgements

I thank W. Herr for suggesting this study and for constant encouragement, F. Ruggiero for a careful reading of the manuscript, and F. Schmidt for a helpful comment. J.-P. Koutchouk first asked me about the importance of long-range collisions at injection.

References

[1] J. Irwin, "Diffusive Losses from SSC Particle Bunches due to Long-Range Beam-Beam Interactions", SSC-223 (1989).

[2] Y. Papaphilippou and F. Zimmermann, "Weak-Strong Beam-Beam Simulations for the LHC," Proc. of the Workshop on Beam-Beam Effects in Large Hadron Colliders — LHC99, Geneva, April 12-17, *CERN-SL-99-039 AP* (1999) (J. Poole and F. Zimmermann eds.); published in Physical Review Special Topics – Accelerators and Beams 2, 104001 (1999).

[3] H. Grote, F. Schmidt, L.H.A. Leunissen, "LHC Dynamic Aperture at Collision", LHC Project Note 197 (1999).

[4] H. Grote, private communication (1999).

[5] F. Schmidt and H. Grote, private communication (2001).

[6] O. Brüning, W. Herr, R. Ostojic, "A Beam Separation and Collision Scheme for IP1 and IP5 at the LHC for Optics Version 6.1," CERN-LHC-Project-Report-315 (1999).

[7] O. Brüning, W. Herr, R. Ostojic, "A Beam Separation and Collision Scheme for IP2 and IP8 at the LHC for Optics Version 6.1," CERN-LHC-Project-Report-367 (2000).

[8] W. Chou and D. Ritson, "Dynamic Aperture Studies During Collisions in the LHC", IEEE PAC 1997, Vancouver (1997).